Alkali doped polyvinyl alcohol/graphene electrolyte for direct methanol alkaline fuel cells

Yun-Sheng Ye [a,b], Ming-Yao Cheng [a], Xiao-Lin Xie [c], John Rick [a], Yao-Jheng Huang [b], Feng-Chih Chang [b,*], Bing-Joe Hwang [a,*]

[a] Department of Chemical Engineering, National Taiwan University of Science and Technology, Taipei, Taiwan
[b] Department of Materials and Optoelectronic Science, Nation Sun Yat-Sen University, Kaohsiung, Taiwan
[c] School of Chemistry and Chemical Engineering, Huazhong University of Science & Technology, Wuhan, China

HIGHLIGHTS

- Alkaline nanocomposites membranes prepared by simple blending process.
- Transport properties of membranes were improved with optimum graphene loadings.
- A significant enhancement of the ionic conductivity for the composite membranes.
- A graphene loading of 1.4 wt% giving a ~73% improvement in tensile strength.

GRAPHICAL ABSTRACT
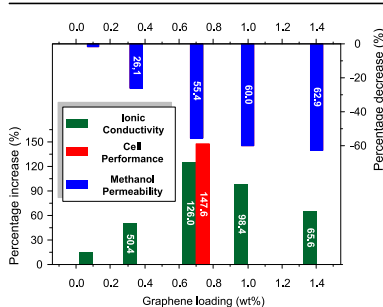
ABSTRACT

Despite the intensive effort directed at the synthesis of anion exchange membranes (AEMs) only a few studies show enhanced ionic conductivity with simultaneous suppression of unfavourable mass transport and improved thermal and mechanical properties. Here we report an alkaline nanocomposite membrane based on fully exfoliated graphene nanosheets and poly(vinyl alcohol) (PVA) prepared by a simple blending process. The composite membrane shows improved ionic transport due to the homogeneous distribution of the graphene nanosheets which are able to form continuous, well-connected ionic channels. Significant enhancement of the ionic conductivity for the prepared graphene/PVA composite membranes is observed with a 0.7 wt% graphene loading resulting in a ~126% improvement in ionic conductivity and a ~55% reduction in methanol permeability. The resulting maximum power density obtained by incorporating the membrane in a cell is increased by ~148%. A higher graphene loading (1.4 wt%) enhances the adhesion of the nanofiller–matrix, giving a ~73% improvement in the tensile strength. This study provides a simple route to designing and fabricating advanced AEMs.

© 2013 Elsevier B.V. All rights reserved.

1. Introduction

Proton exchange membrane fuel cells (PEMFCs) are being developed as a future power generation technology with the potential to deliver clean-at-the-point-of-use power. As well as their environmental friendliness they additionally offer high power densities, high energy conversion efficiencies, and low starting temperatures [1,2]. Although PEMFCs have been widely researched in recent decades and are considered to be an important development, their inherent limitations in acidic conditions, due to: noble metal catalyst poisoning by carbon monoxide at low temperatures, complex water management, limited PEM working lifetime and

* Corresponding authors.
  E-mail address: bjh@mail.ntust.edu.tw (B.-J. Hwang).

high fuel permeability, together with the rarity and consequent high cost of platinum catalysts bring various limitations to PEMFCs [3–5]. In contrast to acidic fuel cells, alkaline fuel cells (AFCs) have several advantages that overcome some of the PEMFC's scientific and technological difficulties. These advantages include: (1) the enhancement of both fuel oxidation and oxygen reduction reaction kinetics, thereby allowing the use of non-noble metal catalysts (e.g. silver, nickel and palladium), (2) the metals suffering less corrosion and are thus more stable in alkaline environments, (3) improved water management, i.e. the electroosmotic drag transports water away from the cathode, and (4) low fuel permeability, due to hydroxide ion transport, from the cathode to the anode [5–9].

The anion exchange membrane (AEM) that plays a crucial role in separating fuel and oxygen (or air) while achieving simultaneous anion transfer is one of the key components in AEMFCs. AEMs have the following requirements: adequate mechanical strength, good thermal and chemical stability and suitable ionic conductivity. To meet such demands, most studies use polymeric materials containing quaternary ammonium groups, e.g. quaternized polysulfone, [10–13] poly(2,6-dimethyl-1,4-phenylene oxide), [14] cardo polyetherketone (PEK-C), [15] poly(phenylene), [16] and radiation-grafted PVDF, ETFT and FEP, [17–19]. Unfortunately, the quaternized polymer is unstable in alkaline media at temperatures above 60 °C and at high KOH concentrations [20,21]. Moreover, there are still some outstanding problems confronting the development of AEMs for AEMFC applications, such as, the chemical stability of the cationic groups attached to the AEMs, the lower conductivity of AEMs compared with PEMs, and their overall cost-effectiveness; thus, the development of cost-effective, easily prepared, high-performance AEMs remains an unmet need.

It is well known that incorporating inorganic fillers into polymer electrolytes can alter and improve their physical and chemical properties [22–25]. In addition, the approach of using carbon nanofillers in the polymer electrolyte fuel cell's membrane has also led to a remarkable improvement in membrane performance – in terms of ionic conductivity, mechanical properties and methanol permeability [26–29]. Membranes modified with these nanosized inorganic/carbon fillers have shown encouraging results in both PEMs and AEMs.

Graphene nanosheets are considered effective polymer fillers and have been incorporated into fuel cell polymer matrices. For example, a Nafion membrane, incorporating 0.5 wt% sulfonated graphene oxide (SGO), showed an enhancement in proton conductivity of ∼66% and a significantly reduced methanol permeability of ∼35% [30]. In our previous study, the incorporation of 0.5 wt% GO/poly(sodium-4-styrenesulfonate) modified graphene (PSS-G) into sulfonated polyimide (SPI) led to a significant improvement in selectivity (proton conductivity/methanol permeability), ∼1.5-fold greater than Nafion 117 and 7-fold greater than pristine SPI at 30 °C, while the tensile strength increased by 76% with the addition of 0.9 wt% of GO [31]. These phenomenon have also been observed in ionic liquid (IL)-based polymer electrolyte membranes with incorporated IL polymer modified graphene [PIL(NTFSI)-G] giving enhancements in ionic conductivity (257.4%) and mechanical properties (345% improvement in tensile strength and a near 25-fold increase in modulus at 150 °C) with a minimal loading of PIL(NTFSI)-G (0.5 wt%) [32]. However, the incorporation of graphene into AEMs has not been previously reported.

One key factor affecting the performance of graphene-based nanocomposite membranes is the dispersion of nanofillers in the polymer matrix. To successfully realize the reinforcing potential of graphene nanosheets, they must be fully exfoliated. GO can be easily dispersed in water; thus, hydrophilic polymers, or water-soluble polymers, are suitable polymer matrices for polymer/

graphene nanocomposites, due to their dispersion properties. Poly(vinyl alcohol) (PVA) is a hydroxyl-rich, water-soluble, biocompatible and non-toxic polymer that is commonly used in fuel cells, drug delivery, coating materials, adhesives etc. [33]. When graphene/GO is well dispersed, at the molecular level, e.g. in PVA, it significantly enhances the resulting material's mechanical properties, thermal stability and electrical conductivity [34–39].

Here, we used a simple technique to prepare graphene/PVA nanocomposite membranes by incorporating GO into a PVA matrix, using water as the processing solvent, followed by hydrazine hydrate reduction, film casting, and finishing by alkaline doping. In these PVA/graphene composite membranes, the graphene nanosheets are uniformly dispersed – resulting in continuous, well-connected tortuous ionic channels. This approach introduces sought after transport behaviour properties into the nanocomposite membranes, e.g. high ionic conductivity, low methanol permeability and low activation energy for ionic conduction. Additionally, the graphene nanosheets exhibit strong interfacial strength with the PVA matrix thereby conferring significantly enhanced mechanical properties.

2. Experimental section
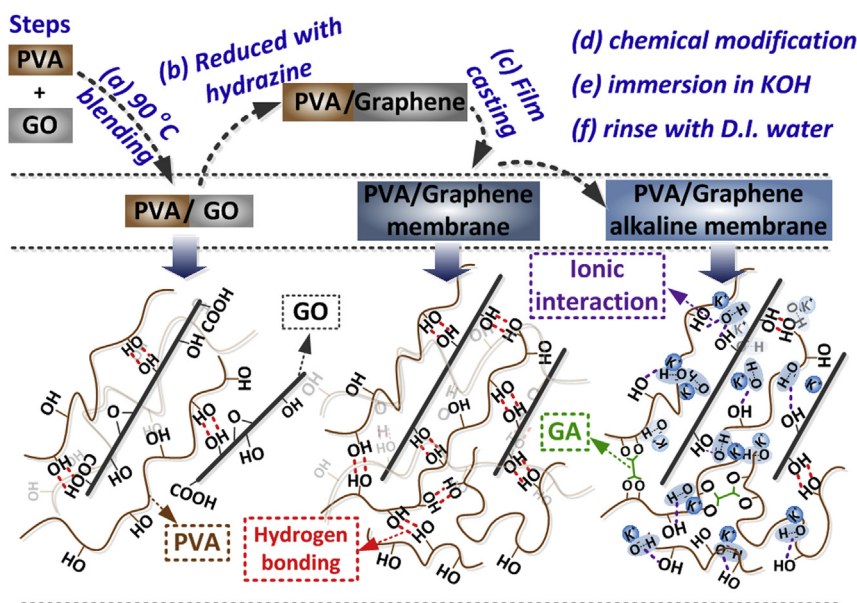
2.1. Composite membrane preparation

Scheme 1 illustrates the preparation of PVA/graphene composite membranes, together with an inner structural model of PVA/graphene, at each stage after doping with KOH solution. PVA powder was dissolved in deionized (D.I.) water at 90 °C in a three-necked flask with mechanical stirring to form an aqueous solution (0.1 g mL^{-1}). GO was prepared according to the method described in our previous study and purified by centrifugation [22,31,32]. The resulting concentrated GO was dilute to 5 mg mL^{-1}. An aqueous GO suspension (5 mg mL^{-1}) was dripped into the PVA solution and stirred at 90 °C for 6 h (step a). The homogeneous dispersion was mixed with a hydrazine solution (mass ratio of hydrazine hydrate:GO = 1:1) and stirred for 1 h at 90 °C (step b). The dispersion was cast onto clean plastic plates at 60 °C for 1 day in a thermal oven to allow film formation (step c). The membrane was peeled-off the plastic plates and soaked in a reaction solution containing 10 mass % glutaraldehyde (GA) (25 wt% solution in water) in acetone at 30 °C for 1 h to give flat membranes [thickness 100–120 μm (step d)]. The thickness of the membranes was able to be well controlled by adjusting the suspension volume.

The preparation of the PVA and PVA/graphene composite membranes was conducted by immersing the membranes in various concentrations of KOH solution at 80 °C for 24 h (step e). The KOH absorbed on the surface of the membranes was removed by repeatedly rinsing in D.I. water (until pH ∼7) after which they were stored in D.I. water at room temperature prior to use (step f).

2.2. Characterization of composite membranes

A DuPont Q100 thermo-gravimetric analyzer (TGA) was used to investigate the thermal stability of the membranes. Samples (∼10 mg) were heated from ambient temperature to 850 °C, under a nitrogen atmosphere, at a heating rate of 20 °C min^{-1}. A tensile strength elongation test was carried out using a universal testing machine (EZ-L-500N; SHIMADZU, Kyoto, Japan). The thicknesses of the test specimens, dimensions 5 mm–50 mm, were measured using a constant crosshead speed of 5 mm min^{-1}.

Crystallization and melting behaviours were investigated by differential scanning calorimetry (DSC). The samples were heated from 30 °C to 150 °C and then maintained at this temperature for 5 min prior to cooling to −30 °C and re-heating to 250 °C. The

Scheme 1. Illustration of PVA/graphene composite membrane synthesis procedure.

heating and cooling rates were 10 °C min^{-1} in all cases. The transition temperatures were taken as the peak maximum in the calorimetric curves. The degree of crystallinity (X_c) was calculated from the following equation:

$$X_c = \Delta H_m / \Delta H_0 \qquad (1)$$

where ΔH_m is taken from the area of the fusion peak. The melting enthalpy of a 100% crystalline PVA, ΔH_0 is taken as 161.6 J g^{-1} [35].

Wide-angle X-ray diffraction (WAXD) 10 spectra were recorded for film samples using a Rigaku D/max-2500 type X-ray diffraction instrument. In order to avoid the influence of the thickness of specimens, all the samples were prepared with a thickness of 100 μm (measured in the dry state). The morphology of the graphene in the composite membranes was observed using a JEOL JEM-1200CX-II transmission electron microscope operated at 120 kV. Scanning electron microscopy (SEM) images were taken with a Hitachi S-4700 microscope using an accelerating voltage of 5–15 kV.

The membrane's alkali uptake (W_a) was calculated from the following equation:

$$W_a = W_t - W_0 / W_0 \qquad (2)$$

where W_0 is the film's dry weight and W_t is the total weight after immersion in either 1 M or 5 M KOH solution.

The membranes' proton conductivities were measured at various temperatures in the wet state. The proton conductivity of the membrane was determined with an ac electrochemical impedance analyzer (PGSTAT30), by scanning from 100 kHz to 10 Hz at a voltage amplitude of 10 mV. The membrane (1 cm in diameter) was sandwiched between two smooth stainless tungsten–copper disk electrodes in a cylindrical PTFE holder placed in a temperature and concentration controlled KOH solution for measurement. At a given temperature, the samples were equilibrated for >30 min before measurement. Repeated measurements were taken at 10 min intervals until no changes in conductivity were observed. The membrane's proton conductivity was calculated from the observed resistance using the relationship:

$$\sigma = L / RA \qquad (3)$$

where L is the proton conductivity (in S cm^{-1}) and L is the distance between the electrodes used to measure the potential ($L = 1$ cm), R is the impedance of the membrane (in Ω), which was measured at the frequency that produced the minimum imaginary response, and A is the membrane section area (in cm^2). The membrane's ionic conductivity, obtained at elevated temperature, can be used to estimate the activation energy (E_a) using the following Eq (1). [23]

$$\ln \sigma = -E_a / RT \qquad (4)$$

where σ is the ionic conductivity in S cm^{-1}, E_a is the activation energy in kJ mol^{-1}, R is the universal gas constant (8.314 J mol^{-1} K), and T is the absolute temperature in K.

The water diffusion coefficient and methanol permeability were determined from methods described in our previous papers [31,40,41]. Water desorption measurements were performed using a TGA Q100 to determine weight changes, over time, at 50 °C. Prior to measurement the test samples were stored in 5 M KOH solution. Methanol permeability measurements for 2 M methanol at 30 °C were carried out on a PVA membrane and PVA/graphene composite. The methanol diffusion coefficient of the membrane was measured using a two-chamber liquid permeability cell. The methanol concentrations in the water cell were determined periodically using a GC-8A gas chromatograph (SHTMADU, Tokyo, Japan). The methanol permeability was calculated using the following Eq. (5):

$$C_B(t) = \frac{A}{V_B} \frac{P}{L} C_A(t - t_0) \qquad (5)$$

where L is the membrane thickness, A is the membrane area, C_A and C_B are the methanol concentrations in the methanol and water chambers, respectively, and P is the methanol diffusion coefficient.

To prepare the AFC electrolytes used in the fuel cell test, PVA and PVA/graphene composite membranes, with 0.7 wt% graphene, were doped with 5 M KOH. A membrane electrode assembly (MEA) was fabricated by sandwiching a composite membrane between two gas diffusion electrodes (E-TEK GDL, LT140EW; 30% Pt on

Vulcan XC-72R, 5 mg cm^{-2}). The MEA was tested in a single cell with a serpentine-shaped gas flow field and an active area of 3 cm^2 at ambient pressure. The power density was calculated as the product of cell voltage and current density (anode: 2 M methanol in 5 M KOH with a flow rate of 5 mL min^{-1}, cathode: humidified oxygen with a flow rate of 100 mL min^{-1}).

3. Results and discussion

3.1. Morphology and structure

It is well known that ionic conductivity and methanol crossover are strongly influenced by the ionic clusters size, connectivity and functional groups. The physical modification of ionic channels by various fillers such as inorganic particles, [42] mesoporous materials, [23] clay or carbon nanotubes [31,41,43] leads to a dramatic decline in methanol crossover due to barrier and molecular sieve effects; moreover, the ionic conductivity may also be increased by the external surface forming three-dimensional ion transport channels. The quality of nanofiller dispersion in the polymer membrane directly correlates with its effectiveness in improving the resulting ionic conductivity, impermeability, and mechanical properties. To disperse the nanosheets into a polymer, GO/PVA was first prepared, followed by the reduction of GO to graphene. The resulting homogeneous PVA/graphene solution was directly cast onto clean plastic plates, and the alkaline membranes were prepared by reaction with KOH as illustrated in Scheme 1 (see Experimental section). The PVA/graphene composite membranes are freestanding and flexible; additionally, they can be easily cut into any desired size or shape.

Fig. 1(a)–(c) is crosssectional FESEM images of pure PVA and PVA/graphene alkaline membranes with graphene nanosheets loadings of 0.7 and 1.4 wt%. The bright regions are attributed to high conductivity graphene deposits. The images demonstrate that most of the graphene nanosheets are fully exfoliated and are clearly well dispersed in the PVA matrix, while there is a limited amount of graphene restacking (black arrows) due to $\pi-\pi$ interactions. Additionally, TEM images, (Fig. 1(d) and (e)) of a PVA/graphene composite membrane, clearly show fully exfoliated graphene nanosheets. The good dispersion and large aspect ratio of the graphene nanosheets results in favourable ion transfer across the PVA/graphene interface, together with unfavourable methanol permeation through the membrane, due to a reduction in cluster size and the enhancement of tortuosity in the composite membrane [30–32]. Also, some agglomerates appear in the PVA/graphene composite membrane, these are attributed to the higher density of graphene loading promoting strong van der Waals interactions between nanolayers, thus increasing the probability of the graphene nanolayers overlapping in the confined space.

PVA is a semi-partially crystalline polymer, with a strong XRD band at $2\theta = 19.4°$ [34,35,39]. Fig. 2(a) shows a small bulge 40.6°, with a large part of the intensity of the composites, i.e. the (101) diffraction peak of PVA crystal at $2\theta = 19.4°$. In addition, a weak peak at $2\theta = 29.4$, 29.4° is attributed to residual KOH in the composite membrane. The intensity of the (101) diffraction peak decreases and becomes wider with increased graphene nanosheet loadings (Table 1), this is reflected in a decrease in crystallinity indicating the occurrence of hydrogen bonding and ionic interactions between the polymer chains, KOH and graphene's oxygenated functionalities.

The polymer matrices' crystallization behaviours in the composite membranes were investigated by DSC, see Fig. 2(b). The parameters derived from the experimental DSC curves are summarized in Table 1, which shows that the melting temperature (T_m) and the melting enthalpy (ΔH_m) are strongly influenced by the
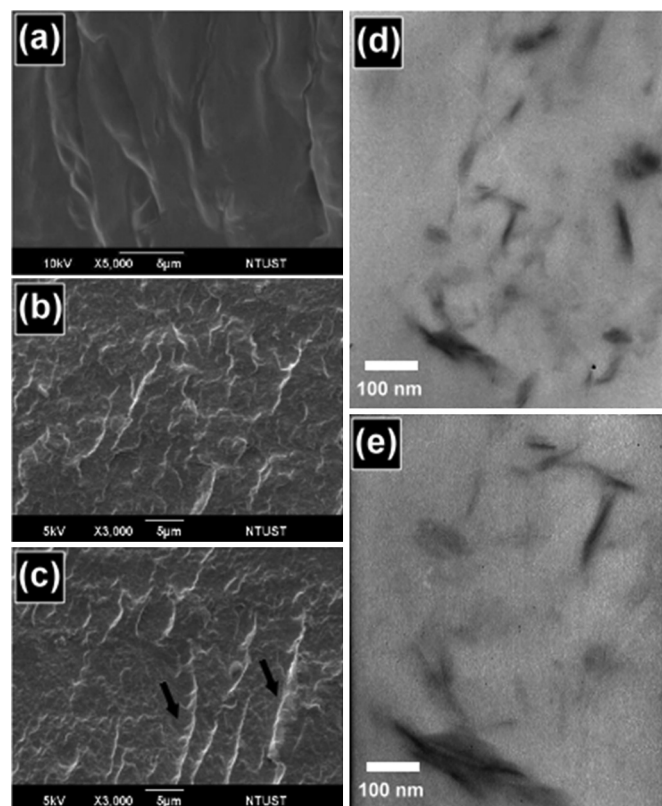

Fig. 1. SEM images of: (a) pure PVA, (b) PVA/graphene 0.7 wt% and (c) 1.4 wt%. TEM images of PVA/graphene (d) 0.7 wt% and (e) 1.4 wt%.

graphene loading. As the graphene loading increases, the melting endotherm of PVA in the composite membrane T_m decreases. In addition, the degree of crystallinity (X_c) of PVA in the composite membranes decreases from 51% to 35% with graphene loadings up to 1.4 wt%. The crystallization change is in good agreement with the XRD result and previous studies [35,37].

3.2. Alkali uptake and methanol solution uptake

The alkali and methanol solution uptakes of AFC membranes are known to have a profound effect on ionic and methanol migration. If dimensional stability can be maintained, the uptake of sufficient water can facilitate a high ionic migration rate. Fig. 3 shows the alkali uptake of the PVA/graphene composite membranes in 1 M and 5 M KOH solution. With the addition of graphene nanosheets into PVA, the alkali uptake first rises (reaching a maximum at 0.1 wt%) and then declines. It was assumed that adding graphene would lead to a decline in the crystallinity of the PVA/graphene composite with an increase in the amorphous region able to accommodate alkali solution, thereby resulting in an increased alkali uptake. However, the alkali uptake does not rise with increases in graphene loading and actually decreases slightly with increasing graphene contents. This may be attributed to a large aspect ratio and the interaction between graphene and the matrix, which restricts alkali induced swelling of the polymer chains. Fig. 3(b) shows that the methanol uptakes of composite membranes with various concentrations of methanol (2–8 M) are much lower than that in alkali solution and decrease with an increase in the graphene content at same methanol concentration. The reduction in methanol solution uptake is attributed to the presence of graphene nanosheets in the membranes which have less affinity to methanol than to water.
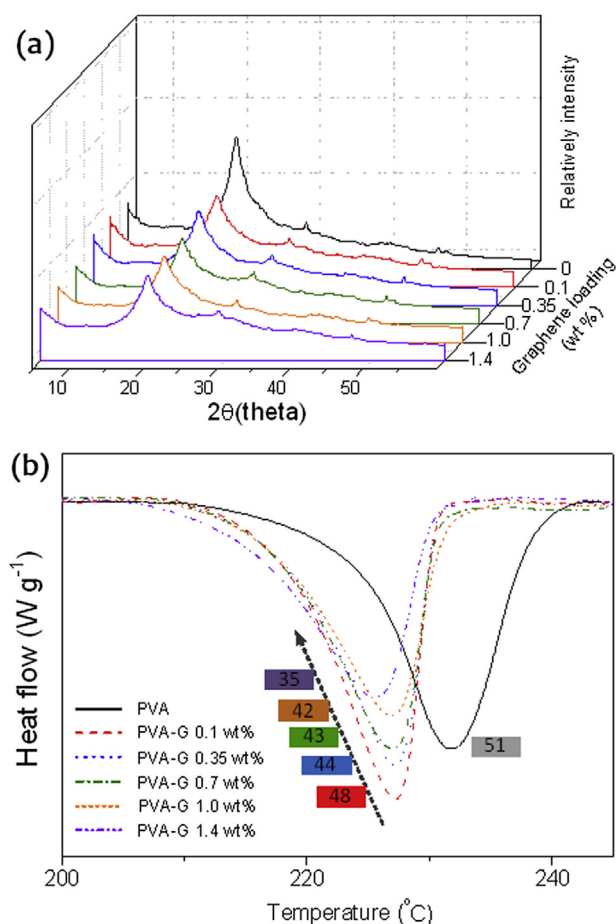
Fig. 2. (a) XRD patterns of PVA–G composite membranes with various weight ratio of graphene. (b) Melting enthalpy of pure PVA and PVA–G composite membranes with various graphene loadings. The numbers in the boxes correspond to the X_c (%).

These results imply that the incorporation of graphene nanosheets into PVA leads to unfavourable methanol swelling due to the creation of a 'methanol barrier'.

Fig. 4 shows the water desorption curves of PVA and PVA/graphene composite membranes. The water diffusion coefficient was markedly reduced with initial increases in the graphene loading from 0.1 to 0.7 wt% and then became less with additional graphene loading. These results indicate that water retention was improved by the introduction of graphene and that the optimum improvement in the composite membrane occurred with a 0.7 wt% graphene loading. This may result from the fully exfoliated graphene layers creating tortuous paths that reduce the transport rate. However, flakes formed on restacking, at higher loadings, lead to weakening and a reduction in tortuosity. The incorporation of clay

Table 1
DSC and XRD data of PVA and PVA/graphene composite.

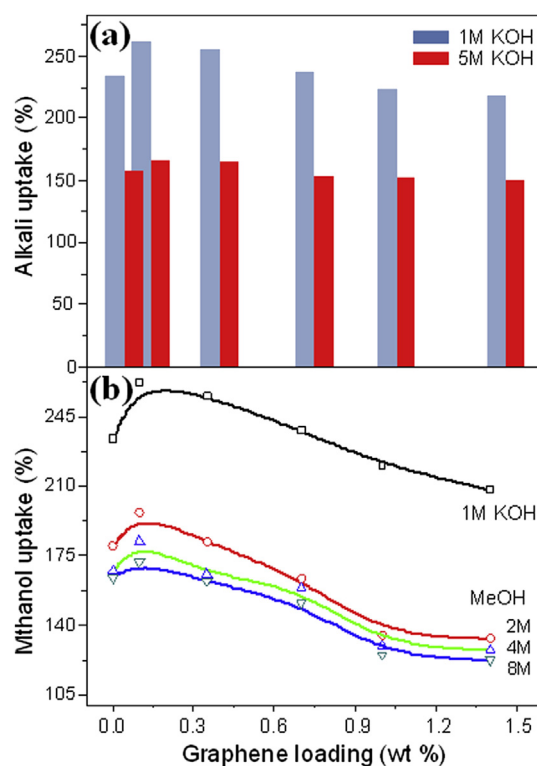| Sample	T_m (°C)	ΔH_m (J g^{-1})	X_c^a (%)	Peak (cps)	Peak width at half height (°)
PVA	232	83	51	2403	2.64
PVA–G 0.1 wt%	227	78	48	1476	2.84
PVA–G 0.35 wt%	227	72	44	1425	3.00
PVA–G 0.7 wt%	227	69	43	1393	3.28
PVA–G 1.0 wt%	226	68	42	1362	3.26
PVA–G 1.4 wt%	225	57	35	1335	3.29

^{a} Calculated from Eq (1).

Fig. 3. The (a) alkali uptake, and (b) methanol uptake of PVA/graphene composite membranes with various weight ratios of graphene.

in other composite membranes has also shown similar results with respect to their water retention properties [41]; such improvements facilitate membrane operation at high temperatures and low relative humidities (RH).

3.3. Ionic conductivity and methanol permeability

The ionic conductivity of the membranes plays an important role in determining the fuel cell's performance. The conductivity of polymer electrolyte membranes is significantly influenced by their water uptake and morphology. The ionic conductivities of the PVA/graphene AFC membranes in 5 M KOH solution at different temperatures (30–80 °C) are shown in Fig. 5 with their relative values being listed in Table 2. The ionic conductivity of the membranes
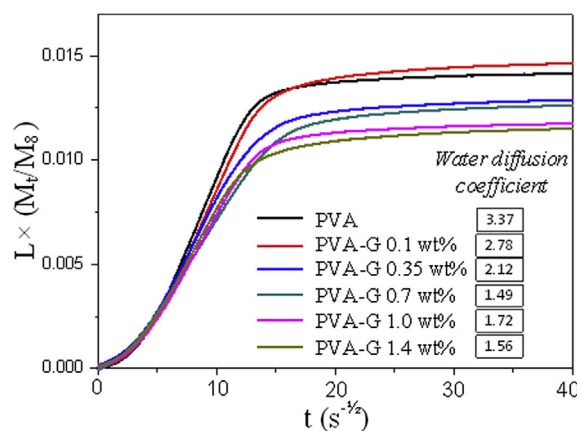

Fig. 4. The water desorption of PVA and PVA/graphene composite membranes. The numbers in the boxes correspond to the water diffusion coefficients ($\times 10^{-7}$ cm^{-2} s^{-1}).
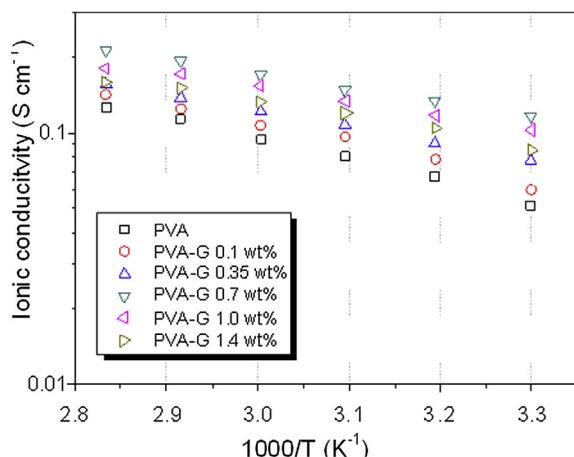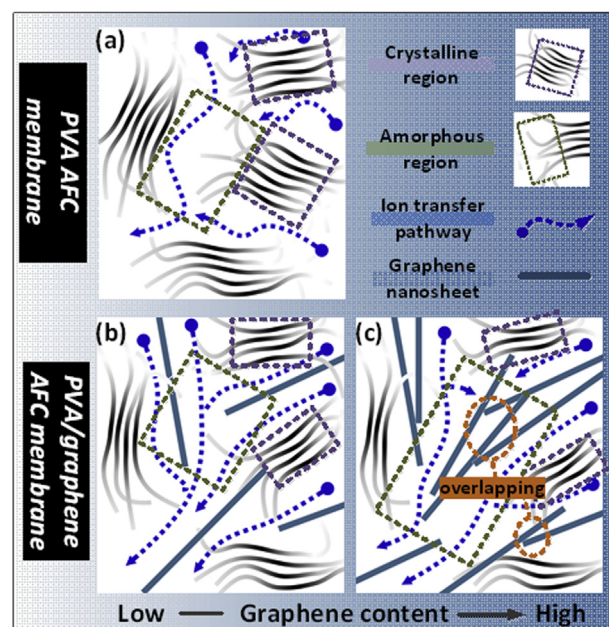
Fig. 5. Ionic conductivities of PVA and PVA/graphene composite membranes plotted as function of inverse temperature.

gradually increases with increasing temperature because the free volume, favouring ion transport and the mobility of anions, is increased as the temperature rises [8,44]. Based on the morphology and water behaviour observation, we have tried to illustrate possible ion transport mechanisms for the PVA and PVA/graphene composite membranes (Scheme 2).

Usually, the ionic conductivity of the polymer electrolyte results from ion transport (hopping between coordinate sites) in the polymer matrix, local structural relaxation and segmental motions of the polymer in amorphous domains as well as ion transport in the solvent. Thus, the decline of crystallinity in PVA/graphene composite membranes (as the XRD and DSC results indicate) facilitates ion transport through the membrane and improves ion transfer. At low graphene loading levels, the homogeneous distribution of graphene sheets as a 3D conductive network through the PVA matrix, in the composite membrane, creates an abundance of interconnected transfer channels. The combination of these two factors may explain the considerable increase in the ionic conductivities of membranes with added graphene. Although, importing more graphene into the PVA matrix creates a higher proportion of amorphous regions, it also causes some parts of the nanosheets to overlap with each other (as the SEM and TEM results indicate) leading to the blocking effect predominating, thus lessening the ionic conductivity improvement.

The effects of morphology changes on the ionic conductivities of the PVA/graphene composite membranes were also observed in the differences in activation energies (E_a). The fitting curve used to calculate the E_a values had temperature boundary conditions of 30 and 80 °C, the values determined are presented in Table 2. The changing trend of E_a values is similar to that of the ionic

Table 2
Transport properties of PVA and PVA/graphene composite membrane.

Sample	Ionic conductivity (10^{-2} S cm^{-1})		Activation energy (E_a) (kJ mol^{-1})[a]	Methanol permeability (10^{-7} cm^2 s^{-1})[b]
	30 °C	80 °C		
PVA	5.2	12.7	15.9	4.28
PVA–G 0.1 wt%	5.9	14.2	14.9	4.21
PVA–G 0.35 wt%	7.8	15.7	12.5	3.16
PVA–G 0.7 wt%	11.7	21.3	10.8	1.91
PVA–G 1.0 wt%	10.3	18.2	10.5	1.71
PVA–G 1.4 wt%	8.6	16.0	11.1	1.59

[a] Calculated from Eq (4).
[b] Calculated from Eq (5).

Scheme 2. Illustration of the ion transport mechanism in the PVA and PVA/graphene composite membranes.

conductivity which is strongly related to the composite membrane's graphene content. This difference reflects the lower energy required for ion transfer through the membrane as importing graphene nanosheets into the polymer electrolyte leads to the formation of well-connected and continuous ionic conductive networks that facilitate ionic movement.

The methanol diffusion coefficients of the PVA and PVA/graphene composite membranes at 30 °C were measured, see Table 2. The methanol diffusion coefficient decreases with increasing graphene loading, from 0.1 to 0.7 wt%, giving at this value, a 55.4% reduction in methanol permeability compared to pure PVA, and thereafter shows a smaller decrement with the addition of excess graphene. This can be attributed to the exfoliated graphene nanosheets reducing the cluster size and enhancing the tortuosity of the composite membrane; however, graphene restacking weakens the tortuosity of the composite membrane [30,31]. Moreover, the lower methanol uptake (see Methanol uptake section) with the incorporation of graphene nanosheets into PVA also contributes to the reduction of methanol permeation. Therefore, we can conclude that the introduction of graphene nanosheets into the PVA AFC membrane can improve ionic conductivity and simultaneously reduce methanol permeation.

3.4. Thermal and mechanical properties

Significantly enhanced mechanical properties are commonly found in polymer/graphene nanocomposites [34,36,45,46]. Fig. 6(a) shows the relationship between the graphene loading and the tensile strength of the composite membranes in the wet and dry states. It is obvious that the addition of graphene into the polymer matrix has a significant influence on its mechanical behaviour. For example, the introduction of graphene (1.4 wt%) results in a maximum increases of 72.9% and 13.3% in the tensile strength for the dry and wet states, respectively. The elongation at break of the composites gradually decreases with graphene loading [Fig. 6(b)]. The value of the elongation at break decreases to 14.4% and 169.3% for the composite with 1.4 wt% loading from 79.7% to 384.9% for pure PVA membrane in the dry and wet states, respectively.
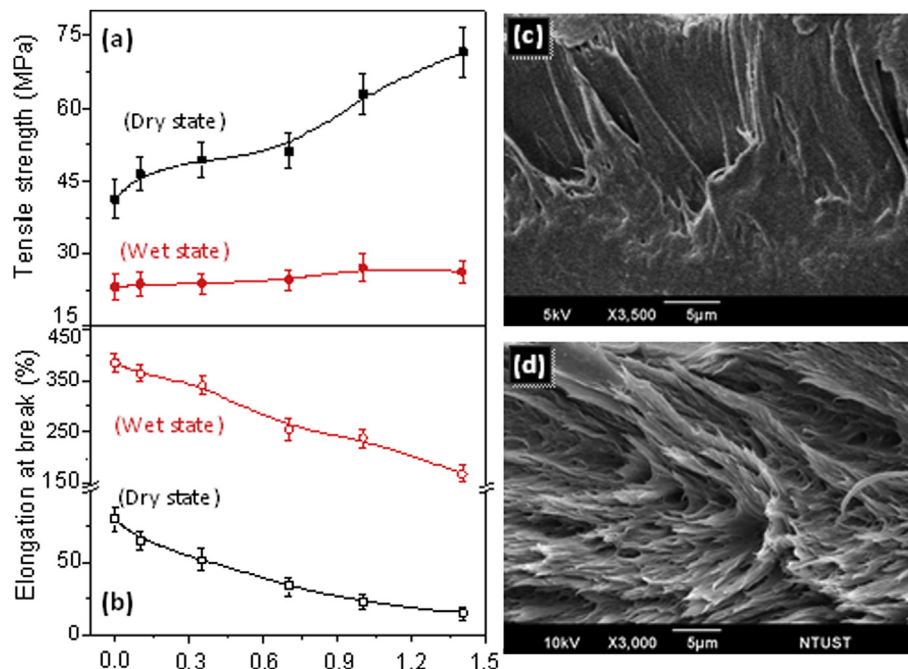
Fig. 6. The (a) tensile strength and (b) elongation at break of PVA and PVA/graphene composite membranes with various weight ratios of graphene. The surface fracture of (c) PVA and (d) PVA/graphene with 0.7 wt% of graphene.

For semi-partially crystalline polymers incorporating PVA, the resulting mechanical properties are strongly dependent on the degree of crystallinity [47]. Although the crystallinity of PVA decreases with increases in graphene loading, mechanical enhancements are not be seriously affected by the poorer crystallinity of PVA/graphene composite membranes. The fact that a good dispersion and a large aspect ratio of graphene nanosheets leads to greater enhancements in the composites membranes' mechanical properties in both the dry and wet states indicates that crystallinity is an important, but not a decisive factor − which can be attributed to the high strength of graphene nanosheets and strong interfacial interactions mediated mainly by hydrogen bonding between the graphene and the PVA matrix.

The fracture surfaces of the PVA and PVA/graphene composite membranes were investigated by SEM after tensile testing. As shown in Fig. 6(c), the pure PVA membrane exhibited a relatively smoother fracture surface than the PVA/graphene composite membrane, indicating a low fracture toughness. In contrast, the fracture surfaces of the composite membrane show considerably different fractographic features [Fig. 6(d)] in that particular orientations of the graphene nanosheets align to the film's surface. As the size and the number of cleavage planes significantly increases, the increased surface roughness implies that the graphene nanosheets contribute to a favourable stress transfer across the graphene/PVA interface, forming a layered-aligned structure on the fracture surface of the PVA/graphene composite membrane.

The thermal stabilities of PVA and PVA/graphene composite membranes were evaluated by TGA with a nitrogen atmosphere, as shown in Fig. 7. In the PVA/graphene composite membranes, there is no obvious increase in thermal stability except for the composite membrane with 1.4 wt% graphene, which is similar to previously reported results [34,36,37,48]. In contrast to other 'layer compounds' e.g. clays which can significantly increase barriers properties by creating a maze or tortuous path within the matrix that retards gas diffusion while enhancing the polymer's thermal properties, the limited enhancement in thermal stability of the

PVA/graphene composite membranes may be attributed to the large heat conductivity of the graphene nanosheets that make it difficult to slow down the heat transfer [39]. However, graphene is still a good physical barrier able to slow down the diffusion of pyrolysis products and gases, as shown by the slowed decomposition in a composite membrane having a 1.4 wt% graphene loading.

3.5. Membrane performance

AFC membranes with high ionic conductivities, low methanol permeabilities and high mechanical properties are desirable for efficient fuel cell operation. Fig. 8 shows that the addition of graphene significantly improves the membrane's ionic conductivity while inhibiting methanol crossover. The PVA/graphene composite membrane, incorporating graphene (0.7 wt%), shows an optimum performance for fuel cell operation and was chosen as the electrolyte for the DMAFCs test. Fig. 9 shows the polarization curves for
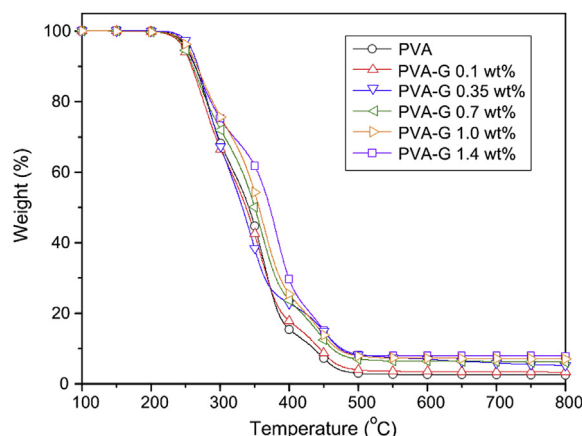

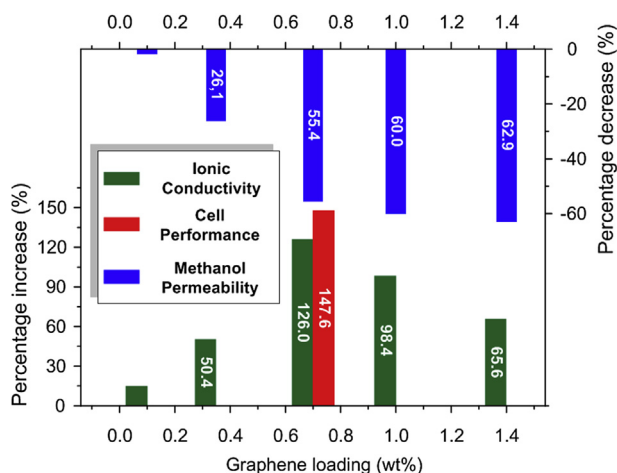**Fig. 7.** TGA curves of PVA and PVA/graphene composite membranes.

Fig. 8. Percentage increase and decrease of PVA/graphene composite membranes incorporated with various weight ratios of graphene.
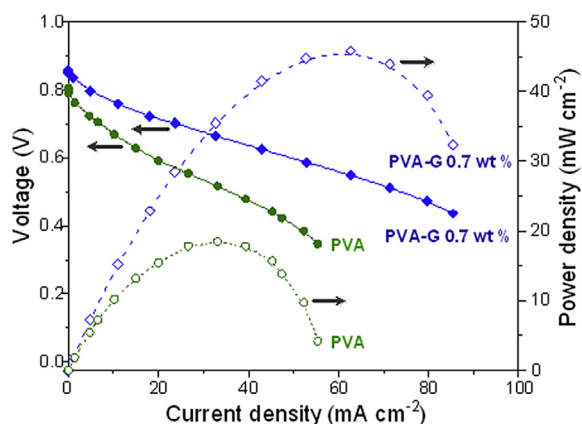

Fig. 9. Polarization curves of DMFC single cells obtained from PVA and PVA/graphene membranes under operating temperature 60 °C.

the DMAFC using the PVA and PVA/graphene electrolytes with 2 M methanol in 5 M KOH at 60 °C. The PVA/graphene membrane exhibited a better performance than the PVA membrane. In particular, the maximum power density value of the PVA/graphene membrane (45.8 mW cm^{-2}) was higher than that of the PVA (18.5 mW cm^{-2}) at 60 °C, corresponding to an increase of 147.6%. The better performance of the PVA/graphene composite membrane can be attributed to selectively facilitated transport, resulting from high ionic conductivity and low methanol crossover.

4. Conclusions

In this work, graphene was incorporated into PVA and the resulting membranes' transport properties were investigated. In these PVA/graphene AFC membranes, the graphene nanosheets were uniformly dispersed resulting in continuous, well-connected and tortuous ionic channels. Such improvements in transport properties result in significant improvements in ionic conductivity (∼126%) and reductions in methanol permeability (∼55%), resulting in a significant enhancement in the cell's performance (∼148% improvement of maximum power density).

Regardless of the improvements in membrane performance, one drawback needing to be addressed is how to avoid the formation of potassium carbonate precipitates during FC operation which

implies that the alkane solution-based system needs to be changed to overcome the presence of potassium. Nevertheless, we believe that the incorporation of graphene nanosheets into AEMs offers a route to modifying the transport properties of membranes as well as to developing polymer electrolyte membranes with high-performance potential for practical fuel cell applications.

References

[1] S.J. Peighambardoust, S. Rowshanzamir, M. Amjadi, International Journal of Hydrogen Energy 35 (2010) 9349–9384.
[2] A.-C. Dupuis, Progress in Materials Science 56 (2011) 289–327.
[3] M.S. Whittingham, T. Zawodzinski, Chemical Reviews 104 (2004) 4243–4244.
[4] M.A. Hickner, H. Ghassemi, Y.S. Kim, B.R. Einsla, J.E. McGrath, Chemical Reviews 104 (2004) 4587–4611.
[5] K.A. Mauritz, R.B. Moore, Chemical Reviews 104 (2004) 4535–4586.
[6] N.J. Robertson, H.A. Kostalik, T.J. Clark, P.F. Mutolo, H.c.D. Abruña, G.W. Coates, Journal of the American Chemical Society 132 (2010) 3400–3404.
[7] W. Li, J. Fang, M. Lv, C. Chen, X. Chi, Y. Yang, Y. Zhang, Journal of Materials Chemistry (2011).
[8] B. Lin, L. Qiu, J. Lu, F. Yan, Chemistry of Materials 22 (2010) 6718–6725.
[9] J.R. Varcoe, R.C.T. Slade, E. Lam How Yee, Chemical Communications (2006) 1428–1429.
[10] M. Tanaka, M. Koike, K. Miyatake, M. Watanabe, Macromolecules 43 (2010) 2657–2659.
[11] J. Wang, S. Li, S. Zhang, Macromolecules 43 (2010) 3890–3896.
[12] S. Gu, R. Cai, T. Luo, Z. Chen, M. Sun, Y. Liu, G. He, Y. Yan, Angewandte Chemie International Edition 48 (2009) 6499–6502.
[13] J. Pan, S. Lu, Y. Li, A. Huang, L. Zhuang, J. Lu, Advanced Functional Materials 20 (2010) 312–319.
[14] Y. Wu, C. Wu, J.R. Varcoe, S.D. Poynton, T. Xu, Y. Fu, Journal of Power Sources 195 (2010) 3069–3076.
[15] Y. Xiong, Q.L. Liu, Q.H. Zeng, Journal of Power Sources 193 (2009) 541–546.
[16] M.R. Hibbs, C.H. Fujimoto, C.J. Cornelius, Macromolecules 42 (2009) 8316–8321.
[17] J.R. Varcoe, R.C.T. Slade, E. Lam How Yee, S.D. Poynton, D.J. Driscoll, D.C. Apperley, Chemistry of Materials 19 (2007) 2686–2693.
[18] H. Herman, R.C.T. Slade, J.R. Varcoe, Journal of Membrane Science 218 (2003) 147–163.
[19] T.N. Danks, R.C.T. Slade, J.R. Varcoe, Journal of Materials Chemistry 13 (2003) 712–721.
[20] H. Hou, G. Sun, R. He, B. Sun, W. Jin, H. Liu, Q. Xin, International Journal of Hydrogen Energy 33 (2008) 7172–7176.
[21] Y. Wang, L. Li, L. Hu, L. Zhuang, J. Lu, B. Xu, Electrochemistry Communications 5 (2003) 662–666.
[22] Y.-S. Ye, Y.-N. Chen, J.-S. Wang, J. Rick, Y.-J. Huang, F.-C. Chang, B.-J. Hwang, Chemistry of Materials (2012).
[23] Y.-S. Ye, G.-W. Liang, B.-H. Chen, W.-C. Shen, C.-Y. Tseng, M.-Y. Cheng, J. Rick, Y.-J. Huang, F.-C. Chang, B.-J. Hwang, Journal of Power Sources 196 (2011) 5408–5415.
[24] F. Pereira, K. Vallé, P. Belleville, A. Morin, S. Lambert, C. Sanchez, Chemistry of Materials 20 (2008) 1710–1718.
[25] S.J. Lue, W.-T. Wang, K.P.O. Mahesh, C.-C. Yang, Journal of Power Sources 195 (2010) 7991–7999.
[26] Y.-L. Liu, Y.-H. Su, C.-M. Chang, Suryani, D.-M. Wang, J.-Y. Lai, Journal of Materials Chemistry 20 (2010) 4409–4416.
[27] S. Yun, H. Im, Y. Heo, J. Kim, Journal of Membrane Science 380 (2011) 208–215.
[28] B.P. Tripathi, M. Schieda, V.K. Shahi, S.P. Nunes, Journal of Power Sources 196 (2011) 911–919.
[29] R. Kannan, B.A. Kakade, V.K. Pillai, Angewandte Chemie 120 (2008) 2693–2696.
[30] B.G. Choi, J. Hong, Y.C. Park, D.H. Jung, W.H. Hong, P.T. Hammond, H. Park, ACS Nano (2011).
[31] C.-Y. Tseng, Y.-S. Ye, M.-Y. Cheng, K.-Y. Kao, W.-C. Shen, J. Rick, J.-C. Chen, B.-J. Hwang, Advanced Energy Materials (2011).
[32] Y.-S. Ye, C.-Y. Tseng, W.-C. Shen, J.-S. Wang, K.-J. Chen, M.-Y. Cheng, J. Rick, Y.-J. Huang, F.-C. Chang, B.-J. Hwang, Journal of Materials Chemistry 21 (2011) 10448–10453.
[33] Y.-S. Ye, J. Rick, B.-J. Hwang, Polymers 4 (2012) 913–963.

[34] J. Liang, Y. Huang, L. Zhang, Y. Wang, Y. Ma, T. Guo, Y. Chen, Advanced Functional Materials 19 (2009) 2297–2302.
[35] H.J. Salavagione, G. Martinez, M.A. Gomez, Journal of Materials Chemistry 19 (2009) 5027–5032.
[36] Y. Xu, W. Hong, H. Bai, C. Li, G. Shi, Carbon 47 (2009) 3538–3543.
[37] X. Yang, L. Li, S. Shang, X.-M. Tao, Polymer 51 (2010) 3431–3435.
[38] X. Zhao, Q. Zhang, D. Chen, P. Lu, Macromolecules 43 (2010) 2357–2363.
[39] C. Bao, Y. Guo, L. Song, Y. Hu, Journal of Materials Chemistry 21 (2011) 13942–13950.
[40] Y.-S. Ye, W.-Y. Chen, Y.-J. Huang, M.-Y. Cheng, Y.-C. Yen, C.-C. Cheng, F.-C. Chang, Journal of Membrane Science 362 (2010) 29–37.
[41] Y.-J. Huang, Y.-S. Ye, Y.-J. Syu, B.-J. Hwang, F.-C. Chang, Journal of Power Sources 208 (2012) 144–152.
[42] G. Gnana Kumar, A.R. Kim, K. Suk Nahm, R. Elizabeth, International Journal of Hydrogen Energy 34 (2009) 9788–9794.
[43] T. Yamaguchi, H. Zhou, S. Nakazawa, N. Hara, Advanced Materials 19 (2007) 592–596.
[44] J.L. Yan, M.A. Hickner, Macromolecules 43 (2010) 2349–2356.
[45] D. Chen, H. Zhu, T. Liu, ACS Applied Materials & Interfaces 2 (2010) 3702–3708.
[46] M.A. Rafiee, J. Rafiee, Z. Wang, H. Song, Z.-Z. Yu, N. Koratkar, ACS Nano 3 (2009) 3884–3890.
[47] M. Cadek, J.N. Coleman, V. Barron, K. Hedicke, W.J. Blau, Applied Physics Letters 81 (2002) 5123–5125.
[48] H. Kaczmarek, A. Podgórski, Polymer Degradation and Stability 92 (2007) 939–946.